Desalination and Water Treatment
www.deswater.com

doi: 10.5004/dwt.2021.27202

225 (2021) 18–28
June

Membrane displaying a dual thin-film titanium-zirconium as selective layers for water treatment

Chabi Noël Worou[a,*], Jing Kang[a], Taofic Bacharou[b], Jimin Shen[a], Pengwei Yan[a], Arcadius Degan[b,c], Yingxu Gong[a], Razack Guene[a], Zhonglin Chen[a,*]

[a]*State Key Laboratory of Urban Water Resource and Environment, School of Environment, Harbin Institute of Technology, Harbin 150090, China, Tel. +8613019005638/+22995525175; email: worouccc@yahoo.fr/worouccc@stu.hit.edu.cn (C.N. Worou), Tel. +8613019718864; emails: zhonglinchen@hit.edu.cn (Z. Chen), jingkanghit@163.com (J. Kang), shenjimin@hit.edu.cn (J. Shen), yanpengwei@stu.hit.edu.cn (P. Yan), Tel. +8618686819519; emails: gyx667@126.com (Y. Gong), razackguenel@gmail.com (R. Guene)*
[b]*Laboratory of Mechanics and Energetics Applied, Polytechnic School of Abomey-Calavi, 01 BP 2009 Cotonou, Benin, Tel. +22995996086; emails: btaofic@yahoo.fr (T. Bacharou)*
[c]*Laboratory of Applied Hydrology, Polytechnic School of Abomey-Calavi, 01 BP:526 INE/UAC, Cotonou, Benin, Tel. +229 96638124/+229 95923751; email: arcdeg01@yahoo.fr (A. Degan)*

Received 20 October 2020; Accepted 3 March 2021

ABSTRACT

A single dual thin-film titanium-zirconium as selective layers membrane for divalent and monovalent ions removal was fabricated. Both dioxide of titanium (TiO_2) and dioxide of zirconium (ZrO_2) have been co-deposited on an ultrafiltration polyacrylonitrile membrane using information given by scanning electron microscopy (SEM) combined with energy-dispersive X-ray spectroscopy (EDS). The important insights provided by SEM associated with EDS on the arrangement and potential functions of nanoparticles (NPs) due to their unambiguous chemical signal were used for characterization and modification of membrane surface at an atomic scale. Thus, a novel thin-film composite-nanofiltration membrane (TFC-NFM) has been performed for the first time. The new-born organic–inorganic membrane NF-TiZr exhibited excellent performance rejection towards monovalent ions and its rejection rate for multivalent ions reached 95%. The order of salts rejection was $CaCl_2$ > $MgSO_4$ ~ $MgCl_2$ > NaCl > Na_2SO_4. The permeate flux of the NF-TiZr membrane is as high as 58 L m^{-2} h^{-1}. 180 h-continuous exploitation of NF-TiZr showed a slight variation of permeate flux less than 1.2% and the salt rejection remained high than 92.5% at the end of the operation. To our best knowledge, it is the first time SEM was combined with EDS to help for optimal co-deposition of nanoparticles on the membrane surface. This study may provide useful insights to design next-generation NFMs.

Keywords: Nanoparticle; Co-deposition; Ions removal; Organic–inorganic membrane; Thin-film composite membranes; Salts rejection

1. Introduction

Among the technologies for wastewater or drinking water purification, nanofiltration (NF) is nowadays one of the most prominent [1–3]. NF technology has quickly acquired the merit of promoting high permeability and low operating pressure [4]. With properties between ultrafiltration (UF) and reverse osmosis (RO), NF is a pressure-driven process that performs the rejection of small organic molecules and multivalent ions. Nowadays, the NF process is used in the fields of beverage production [5], recycled water, and dyes separation [6–9], food and dairy processing [10]. The pore size of nanofiltration membranes

* Corresponding authors.

(NFMs) is about 1 nm and they possess a molecular weight cut-off between 200 and 500 Da [11]. Until now polymeric NFMs exhibit thermal, mechanical stability, and chemical problems [12,13]. These problems are exacerbated by the cost of maintenance and the limited handling conditions in the laboratory [14,15]. Due to these disadvantages of polymeric membranes, ceramic membranes have emerged with high stability, large operating conditions, well-defined pore size, and shape [16].

Several aspects of NFMs have been cleared up in review papers [17,18]. Nghiem et al. [19] have written a comprehensive reference book on nanofiltration. Another recent work covered the chemical modification of NFMs [20], fouling issue [21,22], effects of operating parameters on membrane permeation [23], NF for textile, dye, and wastewater treatment [24], and NF modeling [25]. With the discovery of scanning electron microscopy (SEM) combined with energy-dispersive X-ray spectroscopy (EDS), it is now well established that the elements charge on membrane surface influence the performance of the membrane [26–30].

NF showed a good performance for rejection of divalent ions Mg^{2+}, Ca^{2+}, and SO_4^{2-} from water [31–34]. Recent work on thin-film composite (TFC) membranes coupled with electrodialysis systems for ions (monovalent and divalent) separation has been performed [35,36]. Bazinet and Moalic [35] performed the separation of monovalent cations from seawater using an electrodialysis cell combined with a NF-membrane. In that study, monovalent cations possessed higher flux through the membrane than the multivalent cations. Ge et al. [36] finally compared the performance of a novel in-situ prepared nanofiltration membrane and a commercial membrane (CSO, AGC Eng. Co. Ltd., Cheung Sha Wan Road, Kowloon, Hong Kong) for the separation of sodium and magnesium using the electrodialysis process. The ion flux was calculated from the following equation:

$$J_{M^{n+}} = \frac{\left(C_t - C_0\right)V}{A_m t} \tag{1}$$

where $J_{M^{n+}}$ is the flux of ion M^{n+} (mol cm^{-2} s^{-1}); C_t is the concentration at time t; C_0 is the concentration at time 0 in mol L^{-1}; A_m membrane surface area (cm), and V is the volume in (L).

Thin-film composite-nanofiltration membranes (TFC-NFMs) are the most spread world-wide among the currently available for their encouraging performances that they show. Laboratory experimentations to modify these membranes in order to make them more efficient and more competitive are increasing. Most of the ideal nanofiltration membranes (NFMs) are thin-film composite (TFC) membranes with a substrate and a thin-film selective layer [37–39]. Organic–inorganic TFC-NFMs were prepared by dispersing inorganic fillers in the polymer selective layer through blending, sol–gel method, or in-situ formation [40–44]. To successfully manufacture this type of membrane, a judicious choice of the organic support, of the inorganic nanoparticles (NPs) and a link that would play the role of "bio-glue" for good adhesion between the substrate and the inorganic top layer is essential. In this study as organic substrate, a UF membrane polyacrylonitrile (PAN) also known as Creslan 61 or polyvinyl cyanide has been used; and for inorganic NPs both dioxide of titanium (TiO_2) and dioxide of zirconium (ZrO_2) have been chosen.

So, UF-PAN was hydrolyzed in a sodium hydroxide solution and then immersed into a hydrochloric acid solution in order to prepare its surface to receive a "bio-glue" with great adhesive strength. In this case, dopamine hydrochloride, a well-known bio-glue can be oxidized in an alkaline environment and forms a polymer-like coating on various substrates with great adhesive strength. Yan et al. [37] used in their work polyethyleneimine (PEI) as a crosslinking component to promote the homogeneous polymerization of dopamine and uniform co-deposition of PDA-PEI. In order to avoid this self-aggregation of dopamine and to obtain a smooth and dense selective layer, dopamine hydrochloride (DA) was dissolved in Tris HCl buffer solution. The support that is getting ready can finally receive by a controlled hydrolysis process, the deposition of both titania–zirconia layers as detailed in a forthcoming paragraph. The equilibrium reactions that occur are listed as follows:

- For titania (TiO_2):

$$\left[T_i O\left(SO_4\right)\right] + 3H_2O \rightarrow 2H^+ + \left[T_i\left(OH\right)_4 SO_4\right]^{2-} \tag{2}$$

$$\left[T_i\left(OH\right)_4 SO_4\right]^{2-} \rightarrow T_iO_2 + SO_4^{2-} + 2H_2O \tag{3}$$

- For zirconia (ZrO_2):

$$2\left[Z_r\left(SO_4\right)_2\right] + 3H_2O \rightarrow \left[Z_{r2}\left(OH\right)_3\left(SO_4\right)_4\right]^{3-} + 3H^+ \tag{4}$$

$$\left[Z_{r2}\left(OH\right)_3\left(SO_4\right)_4\right]^{3-} + 3OH^- \rightarrow Z_{r2}\left(OH\right)_6 SO_4 + 3SO_4^{2-} \tag{5}$$

$$Z_{r2}\left(OH\right)_6 SO_4 + 2OH^- \rightarrow 2Z_rO_2 + SO_4^{2-} 4H_2O \tag{6}$$

2. Materials and methods

2.1. Materials

Ultrafiltration membrane of polyacrylonitrile also known as polyvinyl cyanide or Creslan 61 M-U4040 PAN (L = 101.6 cm; l = 96 cm; D = 9.9cm) is a commercial product of Jiangsu Kaimi Membrane Technology Co. Ltd., (China) or available in Shanghai MegaVision Membrane Engineering & Technology Co. Ltd., (China). Dopamine hydrochloride and Tris buffer solutions were purchased from Aladdin (China). Titanium sulfate hydrate, hydrochloric acid solution (12 mol L^{-1}), zirconium sulfate tetrahydrate, ethanol, and sodium hydroxide (NaOH) were all obtained from Sinopharm Chemical Reagent Co., Ltd., (China) and used as received.

2.2. Fabrication of the novel thin-film composite nanofiltration membrane NF-TiZr

UF-PAN was hydrolyzed in sodium hydroxide solution (1.5 mol L^{-1}) for 1 h 30 min at 50°C and then immersed into hydrochloric acid solution (2 mol L^{-1}) for another 1 h 30 min at 30°C. The resulted membrane is called HUFPAN, hydrolyzed polyacrylonitrile ultrafiltration

membrane, Fig. 1. Then, dopamine hydrochloride was dissolved in Tris HCl buffer solution (pH = 8.5; 50 mmol L^{-1}) to prepare a fresh solution for deposition; with a total concentration of 2 mg mL^{-1}, and the deposition time was set at 2 h. These conditions are based on the mass of dopamine HCl/tris buffer solution deposited on the membrane surface and the thickness of the coating layer. The circular pieces of HUFPAN membrane with a diameter of 61 mm were prewetted by ethanol for 30 min, and then transferred into the freshly prepared dopamine Tris HCl buffer solution and shaken at 30°C for 2 h. The as-prepared mussel-inspired platforms were washed by deionized (DI) water several times and dried in an ambient environment. The resulted membrane is called DA-Tris coated platform, Fig. 1. At this last step, two solutions were prepared. Solution 1: titanium sulfate hydrate ($Ti{\cdot}SO_4{\cdot}H_2O$) was dissolved in a hydrochloric solution (45 mmol L^{-1}) with a concentration of 4.5 mmol L^{-1}. Solution 2: zirconium sulfate tetrahydrate ($Zr(SO_4)_2{\cdot}4H_2O$) was dissolved in a hydrochloric solution (45 mmol L^{-1}) with a concentration of 4.5 mmol L^{-1}. Pieces of DA-Tris coated platform membranes were immersed into solution 1 at room temperature (30°C) for 6 h and then transferred into solution 2 under the same conditions (30°C, 6 h). The resulted membrane is called NF-TiZr and the fabrication process is represented in Fig. 1. Three different membranes of this kind have been prepared NF-TiZr2:1, NF-TiZr1:1, and NF-TiZr1:2 respectively while the concentration of Ti is two times, equal or half of the concentration of Zr according to solution 1 and solution 2 concentration. For membrane NF-TiZr2:1, [S1] = 2 × [S2]. For membrane NF-TiZr1:1, [S1] = [S2]; so, membrane NF-TiZr1:1 is the same membrane as NF-TiZr. For membrane NF-TiZr1:2, [S1] = 0.5 × [S2].

2.3. Membrane characterization

Table 1 shows the tools and devices used for membranes characterization. To carry out this part of our work, two instruments have been used much more: scanning electron microscope: Zeiss Sigma 500 (Pittsburgh, Pennsylvania, USA) and spectrometer: OXFORD EDS X-Max 50 (Abingdon – Washington – USA). The details about the phase state of nanoparticles TiO_2 and ZrO_2 films were observed on TFC-NFMs surface; so, the morphological characteristics of the novel prepared nanofiltration membranes were also performed with atomic force microscopy (AFM).

SEM is an electron beam emitted by an electron gun. The electron beam is focused and scanned on the surface of the sample to excite the physical signal. After detection, amplification, and signal processing, a scan is formed to reflect the surface characteristics of the sample image. Scanning electron microscopes mainly include three parts: electro-optical system, vacuum system, signal collection, and image display system.

Each element membrane surface measured through EDS has its X-ray characteristic wavelength. The size of the characteristic wavelength depends on the characteristic energy ΔE released during the energy-level transition. The energy spectrometer uses X-rays of different elements. The characteristics of photon characteristic energy are different for component analysis. Five elements have been identified, carbon, oxygen, nitrogen, titanium, and zirconium.

Dynamic water contact angles measurements were performed with an EasyDrop Instrument (DropMeter A-200 contact angle system (MAIST Vision Inspection & Measurement Co. Ltd., China)) at room temperature using the drop method, in which a drop of water was deposited

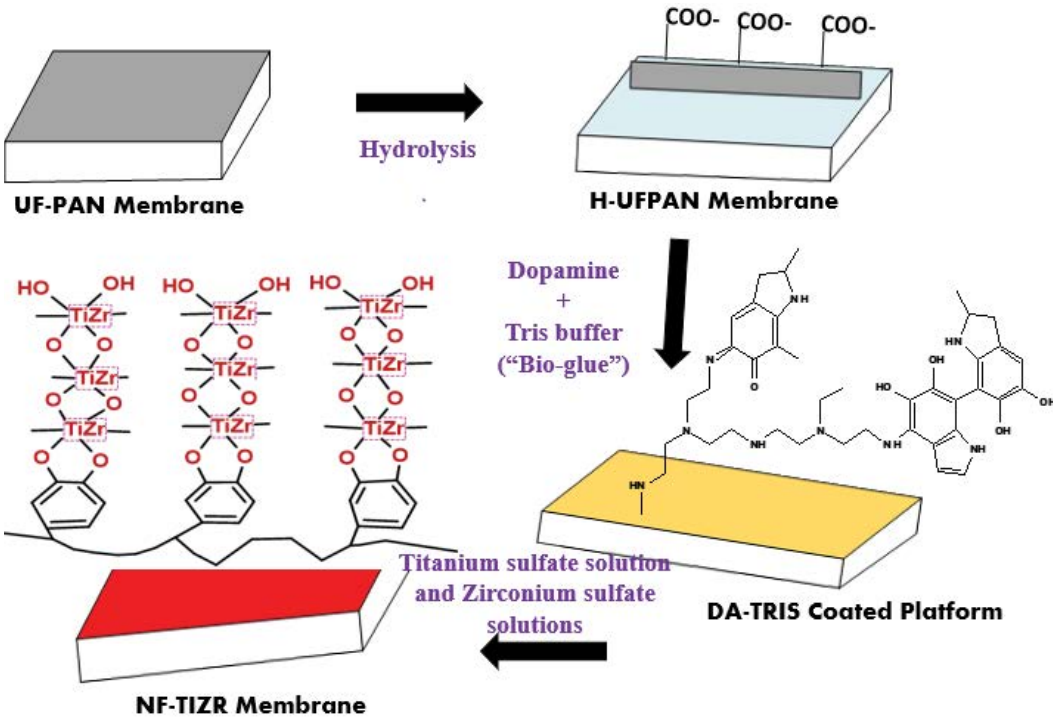

Fig. 1. Novel organic–inorganic nanofiltration membrane NF-TiZr fabrication from an ultrafiltration polymer membrane.

on the surface of a piece of the membrane using a micropipette. The contact angles were measured automatically by a video camera in the instrument using drop shape analysis software. Several measurements on each membrane piece were performed. All membrane pieces were immersed in ethanol for 30 min and dried in an oven prior to measuring their contact angle.

2.4. Membrane performance evaluation

The performance of the novel organic–inorganic NF-TiZr2:1, NF-TiZr1:1, and NF-TiZr1:2 was evaluated by using a laboratory scale cross-flow flat membrane module under 0.6 MPa at 30°C ± 1°C. The effective area was 29.22 cm^2 for each sample. Different salts $MgCl_2$, $CaCl_2$, $MgSO_4$, $NaSO_4$ and NaCl were dissolved in deionized (DI) water at a concentration of 1,000 mg L^{-1} and used as feed solutions with a fixed cross-flow rate of 30 L h^{-1}. The permeate-flux (L_w, L m^{-2} h^{-1}), the pure water permeability (PWP, L m^{-2} h^{-1} bar^{-1}, LMH bar^{-1}) and rejection (R, %) were calculated by Eqs. (7)–(9):

$$F_w = \frac{Q}{At} \tag{7}$$

$$\text{PWP} = \frac{Q}{A\Delta P} \tag{8}$$

where Q, A, ΔP, and t represent the volume of permeated water, the effective membrane area, the trans-membrane pressure, and the permeation time, respectively.

$$R = \left(1 - \frac{C_p}{C_f}\right) \times 100\% \tag{9}$$

where C^p and C^f are respectively the solute concentrations in permeate and feed sides which were measured by a conductivity meter Metrohm AG Grüninger (Ionenstrasse 9100 Herisau, Switzerland) and inductively coupled plasma-optical emission spectroscopy (ICP-OES, Optima 7300 DV, PerkinElmer). All results presented were repeated at least three times. The pieces of organic–inorganic NF-TiZr2:1, NF-TiZr1:1, and NF-TiZr1:2 membranes were tested on the cross-flow flat membrane module for 180 h continuously with measuring the permeate flux and salt rejection every 12 h.

3. Results and discussion

3.1. Energy dispersive spectroscopy of organic–inorganic thin-film composite NF-TiZr2:1, NF-TiZr1:1, and NF-TiZr1:2

In order to get valuable insights into the arrangement and potential functions of nanoparticles TiO_2 and ZrO_2 (NPs) layers coated support, SEM was associated with EDS. Several samples were processed, three were retained as the representative to report on this study. The results of this study are shown in Figs. 2–4 respectively for the membranes NF-TiZr2:1, NF-TiZr1:1 and NF-TiZr1:2. For each membrane, EDS identified five (5) elements carbon (C), oxygen (O), nitrogen (N), titanium (Ti), and zirconium (Zr) due to their unique X-ray signals. Thus, the individual atomic position can be located by its unambiguous chemical signal. The emission light of each atom is not only visible but very distinct from their neighbors due to their high contrast. So, it is possible to characterize and modify the materials at the atomic scale, providing unparalleled insight into the behavior of nanomaterials and particles.

The variation of the concentration ratio had had a remarkable effect on the morphology of the membranes as evidenced by the SEM images of the membranes NF-TiZr2:1, NF-TiZr1:1, NF-TiZr1:2 in Figs. 2b, 3b, and 4b in that order. Although the chemical elements Ti and Zr were uniformly arranged on the three membrane surfaces (Figs. 2e and f, Figs. 3e and f, Figs. 4e and f), there was not necessarily a covalent bond established and ensured between them. But in the case of the NF-TiZr1:1 membrane, this relationship could well be established between the two nanoparticles in use in this study. This view was sustained by the SEM image in Fig. 3b, since the membrane appeared smoother there than in the other two cases. Thus, the surface charge plays a crucial role in organic–inorganic thin-film composite nanofiltration membrane preparation. The performance analysis of the three membranes in the next paragraph will make clear whether it is good or not to necessarily establish a covalent bond between co-deposed nanoparticles or let each nanoparticle act in complete independence.

3.2. Field emission scanning electron microscopy and atomic force microscopy of NF-TiZr2:1, NF-TiZr1:1, and NF-TiZr1:2 membranes

Fig. 5 depicts NF-TiZr2:1, NF-TiZr1:2, and NF-TiZr1:1 membranes' surface morphology and roughness, which are valuable features in the nanofiltration membranes process. All the field emission scanning electron microscopy (FESEM) images are presented with a very high resolution to be able to detect the specificity of each membrane. Operating conditions: precision 200 nm; operating voltage 10.00 kV; working distance 7.8–7.9 mm; magnitude 30.0 KX.

The three organic–inorganic NF membranes belong to the family of thin-film composite membranes (TFC) as depicted very well by their low roughness, 8.00 ± 0.11 nm, 7.13 ± 0.07 nm, and 5.15 ± 0.06 nm respectively for the membranes NF-TiZr2:1, NF-TiZr1:2, and NF-TiZr1:1 since the top-layer deposited on PAN substrate is inferior to 200 nm. Yan et al. [37], for having synthesized a thin layer of zirconium deposited on a UF membrane and obtained a roughness of about 3 nm, qualified the resulted membranes as ultra-thin.

Figs. 5a, c, and e also show at their upper right angle the cross-sectional view of the NF-TiZr2:1, NF-TiZr1:2, and NF-TiZr1:1 membrane respectively. The top TiZr layers with almost invisible pores and a thickness inferior to 10 nm (ultra-thin TFC membranes), which was supported on the bottom layer with larger pores of about 150 nm, has been completely filled with the both titania and zirconia coatings. Furthermore, the cross-section of the NF-TiZr2:1, NF-TiZr1:2, and NF-TiZr1:1 is asymmetric, consisting of loose finger-like macro-voids and interconnecting pores. No distinguishable changes can be observed on the overall cross-sectional morphology among these membranes.

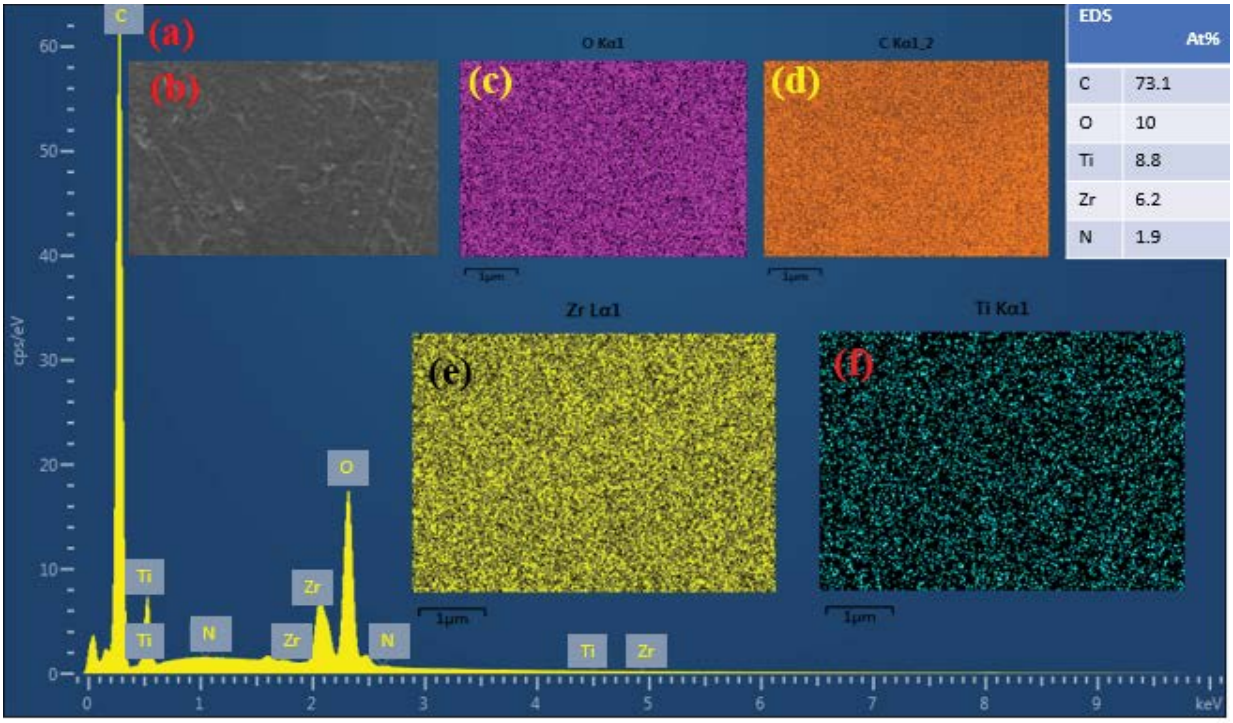

Fig. 2. (a) Energy spectrum analysis results of NF-TiZr2:1 membrane and the sample table surface elements containing (b) scanning electron microscopy (SEM) of NF-TiZr2:1, (c) oxygen, (d) carbon, (e) zirconium, and (f) titanium.

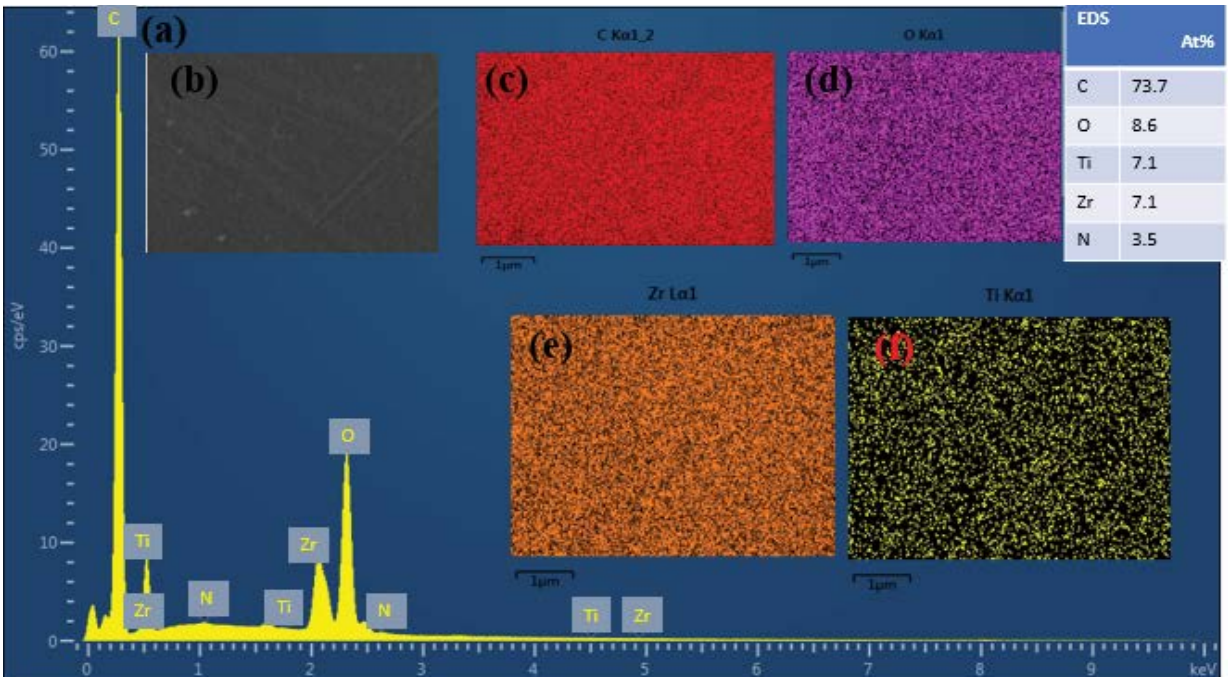

Fig. 3. (a) Energy spectrum analysis results of NF-TiZr1:1 membrane and the sample table surface elements containing (b) scanning electron microscopy (SEM) of NF-TiZr1:1, (c) oxygen, (d) carbon, (e) zirconium, and (f) titanium.

The thinner and more solid the deposited layer is, the more efficient the membrane also is, as observed by Yan et al. [37]. Therefore, a resistant and efficient layer is not necessarily that prepared by a large number of nanoparticles. Hence the still unsuspected importance of the EDS which allows to integrate the distribution of the elements and especially their arrangement on the membrane surface at the atomic scale.

The NF-TiZr1:1 membrane exhibits the most smooth surface. This last feature of the synthesized membrane

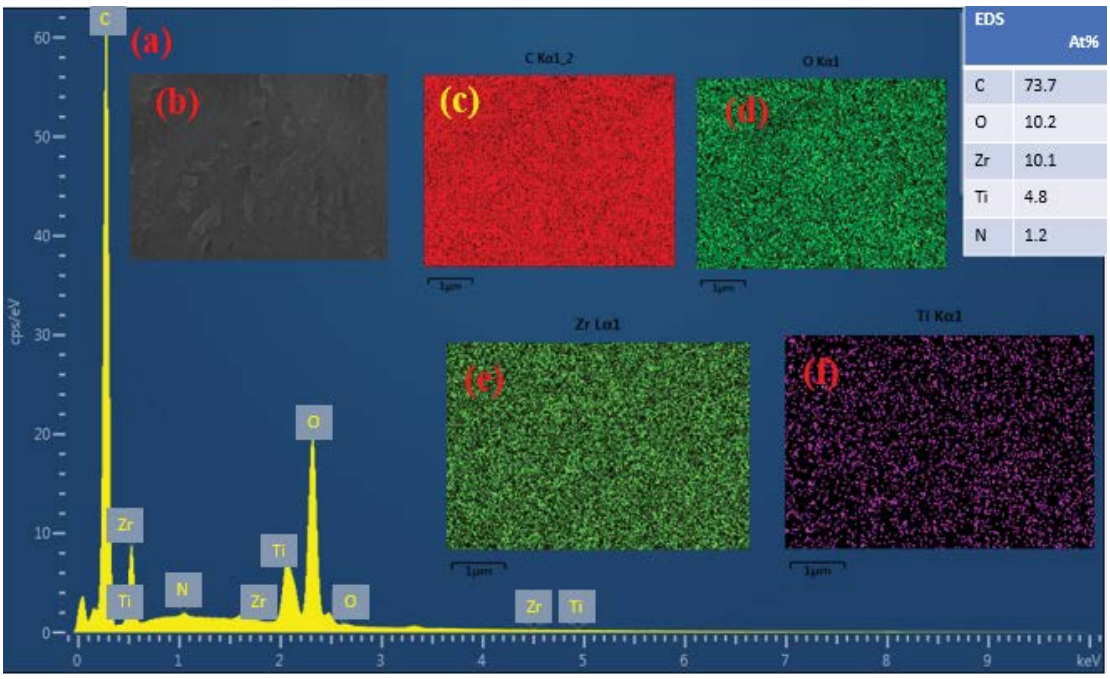

Fig. 4. (a) Energy spectrum analysis results of NF-TiZr1:2 membrane and the sample table surface elements containing (b) scanning electron microscopy (SEM) of NF-TiZr1:2, (c) oxygen, (d) carbon, (e) zirconium, and (f) titanium.

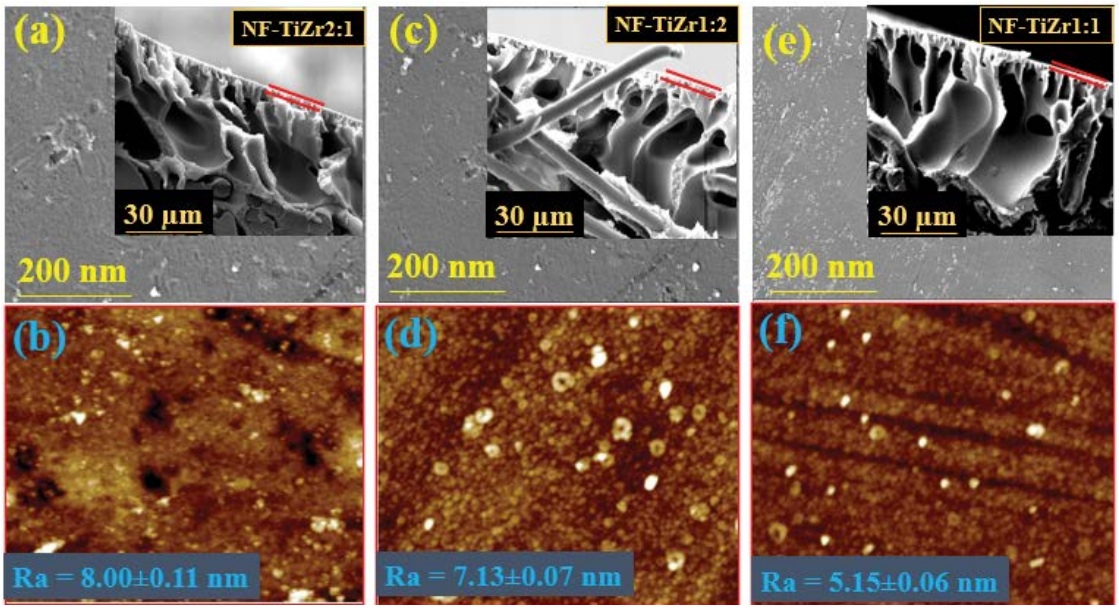

Fig. 5. NF-TiZr2:1 (a and b); NF-TiZr1:2 (c and d); and NF-TiZr1:1 (e and f) membranes FESEM with cross-section and AFM images respectively.

shows that the co-deposition of zirconium and titanium nanoparticles (NPs) is carried out in strict compliance with stoichiometric conditions.

3.3. Surface properties of organic–inorganic thin-film composite NF-TiZr2:1, NF-TiZr1:1, and NF-TiZr1:2

To evaluate the wettability of NF-TiZr2:1, NF-TiZr1:1, and NF-TiZr1:2, a time-dependent water contact angle (WCA) was used to achieve this goal and the results are reported in Fig. 6a. The NF-TiZr1:2 membrane showed the best hydrophilicity and exhibited more zirconium elements (10.1%) on its surface than titanium elements (4.8%), Fig. 4a. The water contact angles of both NF-TiZr2:1 and NF-TiZr1:1 were quite similar from 20 s to the end of the experimentation (100 s). Although almost identical, it was observed that the WCA of the NF-TiZr1:1 membrane was every second below that of the NF-TiZr2:1 membrane.

It could therefore be concluded that under the same handling conditions, the zirconium layer membranes show greater hydrophilicity than the titanium layer membranes. In fact, the three novels TFC-NFM exhibit good hydrophilicity and can be fast spread out by water, which is good for their permeation performance.

Fig. 6b is about the zeta potentials of the novel membranes understudy at various pH values. Between pH 3 and 6, NF-TiZr2:1, NF-TiZr1:1, and NF-TiZr1:2 membranes were positively charged; but during the nanofiltration process conducted above pH = 6, these organic–inorganic TFC-NFMs were negatively charged. For that reason, the pH has been set at 6 as an operating pH condition. TiO_2 and ZrO_2 nanoparticles seem to possess the same influence on membrane electronegativity since NF-TiZr2:1 and NF-TiZr1:2 graphs were quite similar. However, for acid pH (between 3.0 and 5.5) the membrane NF-TiZr2:1 is more electropositive than NF-TiZr1:2. And for pH less acid (pH > 5.5), NF-TiZr2:1 showed the best electro positivity. These slight differences could be explained by the fact that titanium ions can present the two forms Ti^{2+} and Ti^{4+}, whereas we only know Zr^{4+}. Still, the graph of NF-TiZr1:1 as in the case of WCA was sandwiched between the graphs NF-TiZr2:1 and NF-TiZr1:2.

3.4. Performance evaluation of organic–inorganic thin-film composite NF-TiZr2:1, NF-TiZr1:1, and NF-TiZr1:2

The three membranes made from a UF membrane during this experiment, like other NFMs, NFMs were applied to separate ions with different valences from water. The retention performance of salts can reflect the charge characteristics of membranes as suggested by Yan et al. [37]. Thus, in this section, various salt solutions (with a concentration of 1,000 mg L^{-1}) were used to evaluate the rejection performance of the novel organic–inorganic TFC-NFMs. The permeate flux and salt rejection of NF-TiZr2:1, NF-TiZr1:1, and NF-TiZr1:2 membranes towards $MgSO_4$, $MgCl_2$, $CaCl_2$, Na_2SO_4 and NaCl were shown in Fig. 7. The rejection ratio reaches as high as 96% for bivalent cations although it is lower than 20% for monovalent cations. Salts rejection order for NF-TiZr1:1 is $CaCl_2$ > $MgSO_4$ = $MgCl_2$ > NaCl > Na_2SO_4 as represented in Fig. 7a. NF-TiZr2:1 was proficient in rejection of $MgCl_2$ (more than 92%) and NF-TiZr1:2 was proficient towards $CaCl_2$ rejection (about (90%) but worthless towards both Na_2SO_4 and NaCl. The results as presented here, although not so good for the two membranes NF-TiZr2:1 and NF-TiZr1:2 all satisfied those of nanofiltration processes mainly determined by Donnan and dielectric effects [45]. NF-TiZr1:1 exhibited the highest rejection both towards divalent cations (between 89%–95%) and monovalent cations (>60%). This last membrane (NF-TiZr1:1) is a good candidate for monovalent and divalent ions rejection in the water treatment process since it combined the proven efficacity of NPs TiO_2 and ZrO_2 acting separately in membranes selective layers. As demonstrated, the novel organic–inorganic TFC-NFMs are positively charged at pH 6.0 (Fig. 6b) and hence possess a better rejection of multivalent cations than anions (Fig. 6b). The permeate flux during the experimentation didn't change too much and was set at 45, 60, and 58 L $m^{-2}h^{-1}$ respectively for NF-TiZr2:1, NF-TiZr1:2, and NF-TiZr1:1.

Since titanium is thinner than zirconium, membranes synthesized with increased titanium tend to be less permeable but more efficient at forming a barrier for solute particles of the feed solution to pass through the active layer of the membrane and end up in the permeate. On the other hand, NF-TiZr1:2 is more loose and less efficient for salts rejection in the polar opposite of NF-TiZr2:1. NF-TiZr1:1 The NF-TiZr1:1 membrane plays the role of balance while reconciling the advantages of the first two membranes. This state of affairs is understandable, coarse elements tend to create voids while fine elements tend to break. Taken together and well sorted, the fine elements tend to plug the voids left by the large elements and to generate a more solid structure.

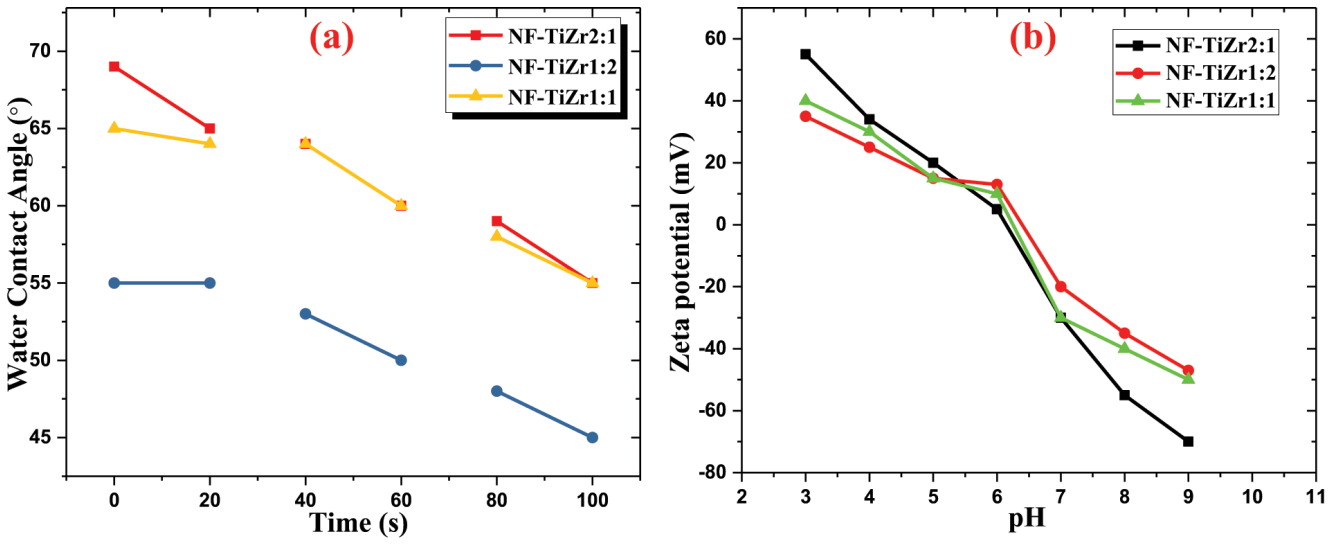

Fig. 6. Water contact angle (a) zeta potential at various pH (b) of NF-TiZr2:1, NF-TiZr1:1, and NF-TiZr1:2 membranes.

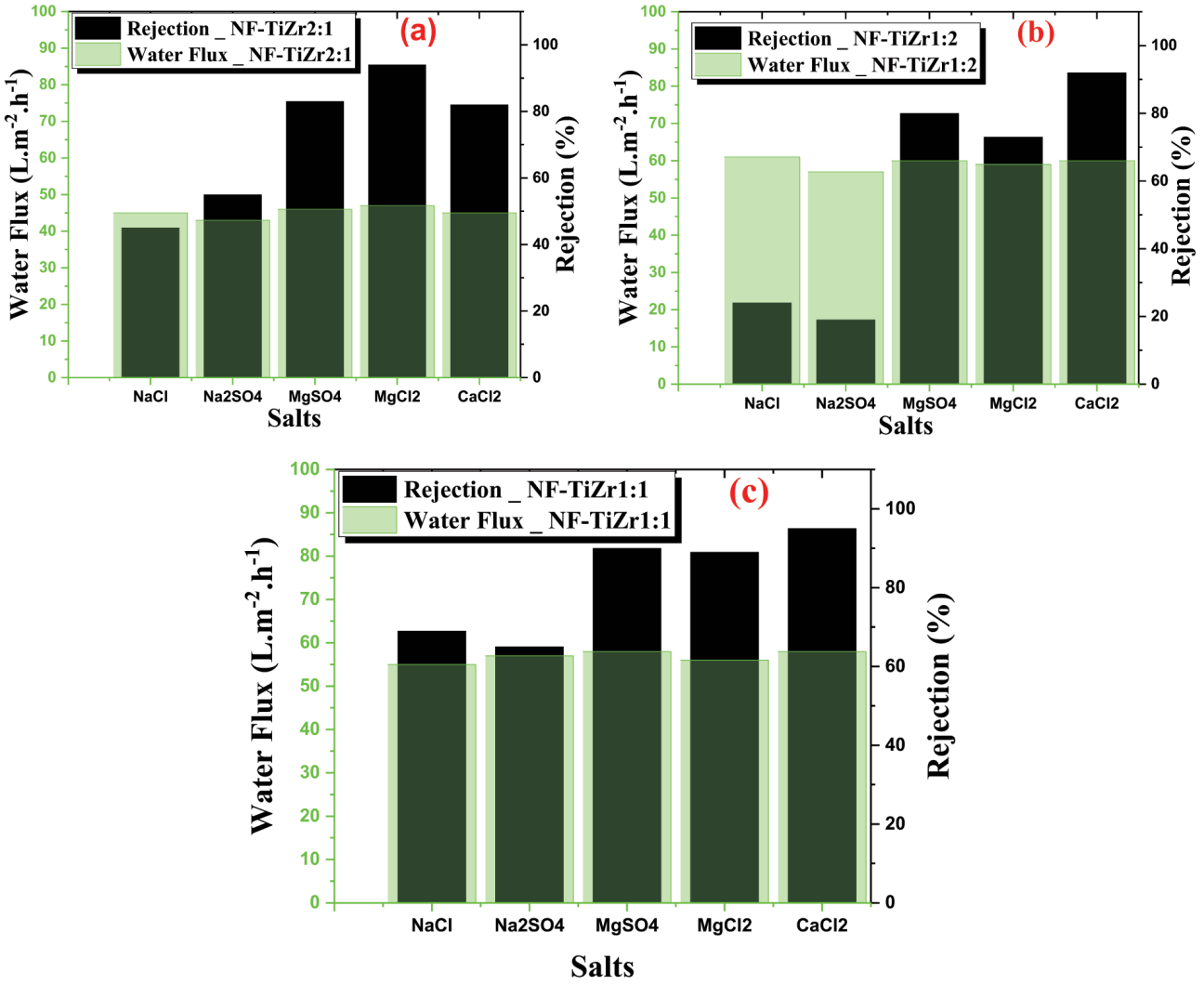

Fig. 7. Different salts rejection of the novel fabricated organic–inorganic thin composite membranes (a) NF-TiZr2:1 (b) NF-TiZr1:2 and (c) NF-TiZr1:1. Operating conditions: pressure = 0.6 MPa; cross-flow rate = 30 L h^{-1}; T = 30°C; pH = 6.0 [$CaCl_2$] = 1,000 mg L^{-1}.

Table 1
Tools and devices used for membranes characterization

Devices	Role
Field emission scanning electron microscopy (FESEM)	Characterize the morphologies of the membranes
Energy-dispersive X-ray spectroscopy (EDS) (Hitachi S-4800, Japan)	Characterize the elemental distribution of the membranes and phase state of TiO_2 and ZrO_2 film
DropMeter A-200 contact angle system (MAIST Vision Inspection & Measurement Co. Ltd., China)	Measure the dynamic water contact angles
Electrokinetic Analyzer (SurPASS Anton Paar GmbH, Austria)	Detect the charging property of the membrane surface

The synthesized membrane (NF-TiZr1:1) permeate flux and rejection performance have been reported in Table 2 below with those of some earlier reported ones.

The membrane synthesized in this study, although very loose, is effective at removing multivalent ions. The permeate flux and the rejection are the two main parameters that help to decide whether an NF membrane is efficient or not [16]. Most often if NF membrane exhibits high permeate flux it is less selective and conversely if it displays excellent rejection it has a low permeate flux release.

Recently, Xu et al. [46] reported a high flux NF membrane based on layer-by-layer assembly modified electrospun nanofibrous substrate, the experiments results

Table 2
Synthesized membrane permeate flux and rejection performance in this study and some earlier reported ones

Membrane	Permeate flux (L m^{-2} h^{-1})	Rejection (%)	References
PAN/ZrO_2–TiO_2 (1:1)	58	92.5	This study
Polyethersulfone/LbL nanofibrous	75	80	[46]
Hydrolyzed-polyacrylonitrile/ZrO_2	60	>90	[37]
Modified membrane (0.5–Ach)	30	95	[47]
PES/TiO_2	4.2	81.9	[48]
PES/functionalized multi-walled carbon nanotubes	24	80	[49]
PES/graphene oxide	20.4	96	[50]
Graphene oxide polyamide	42	90	[51]
TFC-NF/fuctionalized chitosan	22.9	90.8	[52]

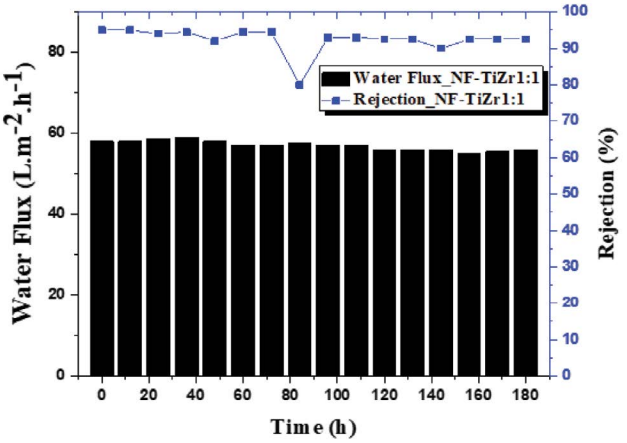

Fig. 8. Long term stability test on NF-TiZr1:1 membrane. Test conditions: pressure = 0.6 MPa; cross-flow rate = 30 L h^{-1}; T = 30°C; pH = 6.0 [$CaCl_2$] = 1,000 mg L^{-1}.

indicated that the resulted membranes exhibited high permeate flux close to 75 L m^{-2} h^{-1} with $MgSO_4$ rejection of 80%.

3.5. Long-term stability test on organic–inorganic thin-film composite NF-TiZr1:1

To evaluate the long-term stability of NF-TiZr1:1, a continuous 180 h-test filtration was carried out. And the results were presented in Fig. 8. Test conditions: concentration (1,000 mg L^{-1}) of $CaCl_2$, 30°C, pH = 6.0, 0.6 MPa, cross-flow rate = 30 L h^{-1}. Globally, both permeate flux and rejection satisfied the long-term stability test. The permeate flux of NF-TiZr1:1 at the start of the experiment was 58 L m^{-2} h^{-1} and the end of the 180 h-test was 56 L m^{-2} h^{-1}. The permeate flux has decreased steadily but very slightly with two anomalies observed at 36 and 84 h. The same anomaly was noted, but in an increased manner at the level of the salt rejection graph at 84 h. This sudden and singular drop in the salt rejection rate could only be explained by a bad reading or that the operator was not on standby. The permeate flux decreased by about 1% during the 180 h-test. The rejection decreased from 95% to 92.5% in 180 h continuous work. Thus, the rejection rate decreased by about 1.4% during the 180 h-test. These results are very encouraging with regard to those obtained recently by Song et al. [53] on titanium-based sol-gel deposition principle and Yan et al. [37] on zirconium using the *in-situ* formation approach. Note that these low depreciation rates (1% for permeate flux and 1.4% for rejection) could be further improved again on the downside if the work was not continuous. Hence, the importance of maintenance work and regular cleaning of the membranes.

4. Conclusion

Both dioxide of titanium (TiO_2) and dioxide of zirconium (ZrO_2) have been co-deposited on ultrafiltration PAN membrane using information given by FESEM combined with EDS. Thus, a novel TFC-NFM has been performed for the first time. NF-TiZr exhibited high-performance rejection towards monovalent ions and the rejection rate for multivalent ions reached 95%. The permeate flux of this organic–inorganic nanofiltration membrane is as high as 58 L m^{-2} h^{-1}. A 180 h continuous exploitation of NF-TiZr demonstrated its long-term operability. Of observation, NF membranes that perform well in ions rejection have low permeate flux. The co-deposition of nanoparticles in strict compliance with stoichiometric conditions seems to improve the flux of such membranes while being very efficient at rejecting ions. We, therefore, recommend that henceforth the scientific world lean much more over NPs co-deposition for a new generation of NF membranes more efficient in terms of rejection and flux release.

References

[1] M. Elimelech, W.A. Phillip, The future of seawater desalination: energy, technology, and the environment, Science, 333 (2011) 712–717.
[2] Y.T. Chua, C.X.C. Lin, F. Kleitz, X.S. Zhao, S. Smart, Nanoporous organosilica membrane for water desalination, Chem. Commun., 49 (2013) 4534–4536.
[3] C.N. Worou, J. Kang, J. Shen, A. Degan, P.W. Yan, W.Q. Wang, Y.X. Gong, Z.L. Chen, Euler's numerical method for ions rejection reassessment of a defect-free synthesized nanofiltration membrane with ultrathin titania film as the selective layer, Coatings, 11 (2021) 184, doi: 10.3390/coatings11020184.
[4] M.X. Chen, C.F. Xiao, C. Wang, H.L. Liu, N.Z. Huang, Preparation and characterization of a novel thermally stable

thin film composite nanofiltration membrane with poly (m-phenyleneisophthalamide) (PMIA) substrate, J. Membr. Sci., 550 (2018) 36–44.
[5] S. Benedetti, E.S. Prudêncio, J.M.G. Mandarino, K. Rezzadori, J.C.C. Petrus, Concentration of soybean isoflavones by nanofiltration and the effects of thermal treatments on the concentrate, Food Res. Int., 50 (2013) 625–632.
[6] S. Yu, M.H. Liu, M. Ma, M. Qi, Z.H. Lü, C.J. Gao, Impacts of membrane properties on reactive dye removal from dye/salt mixtures by asymmetric cellulose acetate and composite polyamide nanofiltration membranes, J. Membr. Sci., 350 (2010) 83–91.
[7] A.Y. Zahrim, C. Tizaoui, N. Hilal, Coagulation with polymers for nanofiltration pre-treatment of highly concentrated dyes: a review, Desalination, 266 (2011) 1–16.
[8] P.S. Zhong, N. Widjojo, T.-S. Chung, M. Weber, C. Maletzko, Positively charged nanofiltration (NF) membranes via UV grafting on sulfonated polyphenylenesulfone (sPPSU) for effective removal of textile dyes from wastewater, J. Membr. Sci., 417 (2012) 52–60.
[9] S. Darvishmanesh, J. Degrève, B. Van der Bruggen, Performance of solvent-pretreated polyimide nanofiltration membranes for separation of dissolved dyes from toluene, Ind. Eng. Chem. Res., 49 (2010) 9330–9338.
[10] F. Salehi, Current and future applications for nanofiltration technology in the food processing, Food Bioprod. Process., 92 (2014) 161–177.
[11] A.W. Mohammad, Y.H. Teow, W.L. Ang, Y.T. Chung, D.L. Oatley-Radcliffe, N. Hilal, Nanofiltration membranes review: recent advances and future prospects, Desalination, 356 (2015) 226–254.
[12] L.F. Greenlee, D.F. Lawler, B.D. Freeman, B. Marrot, P.J. Moulin, Reverse osmosis desalination: water sources, technology, and today's challenges, Water Res., 43 (2009) 2317–2348.
[13] A. Lee, J.W. Elam, S.B. Darling, Membrane materials for water purification: design, development, and application, Environ. Sci. Water Res. Technol., 2 (2016) 17–42.
[14] T. Tsuru, Inorganic porous membranes for liquid phase separation, Sep. Purif. Methods, 30 (2001) 191–220.
[15] M. Gryta, Fouling in direct contact membrane distillation process, J. Membr. Sci., 325 (2008) 383–394.
[16] T.A. Siddique, N.K. Dutta, N.R. Choudhury, Nanofiltration for arsenic removal: challenges, recent developments, and perspectives, Nanomaterials, 10 (2020) 1323, doi: 10.3390/nano10071323.
[17] N. Hilal, H. Al-Zoubi, N.A. Darwish, A.W. Mohammad, M. Abu Arabi, A comprehensive review of nanofiltration membranes: treatment, pretreatment, modelling, and atomic force microscopy, Desalination, 170 (2004) 281–308.
[18] B. Van der Bruggen, M. Mänttäri, M. Nyström, Drawbacks of applying nanofiltration and how to avoid them: a review, Sep. Purif. Technol., 63 (2008) 251–263.
[19] N.D. Nghiem, A.I. Schafer, M. Elimelech, Pharmaceutical retention mechanisms by nanofiltration membranes, Environ. Sci. Technol., 39 (2005) 7698–7705.
[20] B. Van der Bruggen, Chemical modification of polyethersulfone nanofiltration membranes: a review, J. Appl. Polym. Sci., 114 (2009) 630–642.
[21] A.S. Al-Amoudi, Factors affecting natural organic matter (NOM) and scaling fouling in NF membranes: a review, Desalination, 259 (2010) 1–10.
[22] C.Y. Tang, T.H. Chong, A.G. Fane, Colloidal interactions and fouling of NF and RO membranes: a review, Adv. Colloid Interface Sci., 164 (2011) 126–143.
[23] J. Luo, Y. Wan, Effects of pH and salt on nanofiltration—a critical review, J. Membr. Sci., 438 (2013) 18–28.
[24] W.J. Lau, A.F. Ismail, Polymeric nanofiltration membranes for textile dye wastewater treatment: preparation, performance evaluation, transport modelling, and fouling control—a review, Desalination, 245 (2009) 321–348.
[25] D.L. Oatley-Radcliffe, S.R. Williams, M.S. Barrow, P.M. Williams, Critical appraisal of current nanofiltration modelling strategies for seawater desalination and further insights on dielectric exclusion, Desalination, 343 (2014) 154–161.
[26] M. Sbaı, P. Fievet, A. Szymczyk, B. Aoubiza, A. Vidonne, A. Foissy, Streaming potential, electroviscous effect, pore conductivity and membrane potential for the determination of the surface potential of a ceramic ultrafiltration membrane, J. Membr. Sci., 215 (2003) 1–9.
[27] I.H. Huisman, G. Trägårdh, C. Trägårdh, A. Pihlajamäki, Determining the zeta-potential of ceramic microfiltration membranes using the electroviscous effect, J. Membr. Sci., 147 (1998) 187–194.
[28] W.R. Bowen, H. Mukhtar, Characterisation and prediction of separation performance of nanofiltration membranes, J. Membr. Sci., 112 (1996) 263–274.
[29] N. Hilal, H. Al-Zoubi, N.A. Darwish, A.W. Mohammad, Characterisation of nanofiltration membranes using atomic force microscopy, Desalination, 177 (2005) 187–199.
[30] Y.R. Qiu, J. Qi, Electrokinetic characterization of poly(vinyl butyral) hollow fiber membranes by streaming potential and electroviscous effect, J. Membr. Sci., 425 (2013) 71–76.
[31] M. Telzhensky, L. Birnhack, O. Lehmann, E. Windler, O. Lahav, Selective separation of seawater Mg^{2+} ions for use in downstream water treatment processes, Chem. Eng. J., 175 (2011) 136–143.
[32] O. Lehmann, O. Eckhaus, O. Lahav, L. Birnhack, Replenishing Mg(II) to desalinated water by seawater nanofiltration followed by magnetic separation of $Mg(OH)_{2(s)}Fe_3O_4$ particles, Desal. Water Treat., 57 (2016) 19903–19916.
[33] P. Nativ, L. Birnhack, O. Lahav, DiaNanofiltration-based method for inexpensive and selective separation of Mg^{2+} and Ca^{2+} ions from seawater, for improving the quality of soft and desalinated waters, Sep. Purif. Technol., 166 (2016) 83–91.
[34] A.F.M. Alsayed, M.A. Ashraf, Modified nanofiltration membrane treatment of saline water: a review, Desal. Water Treat., 187 (2020) 93–105.
[35] L. Bazinet, M. Moalic, Coupling of porous filtration and ion-exchange membranes in an electrodialysis stack and impact on cation selectivity: a novel approach for sea water demineralization and the production of physiological water, Desalination, 277 (2011) 356–363.
[36] L. Ge, B. Wu, Q.H. Li, Y.Q. Wang, D.B. Yu, L. Wu, J.F. Pan, J.B. Miao, T.W. Xu, Electrodialysis with nanofiltration membrane (EDNF) for high-efficiency cations fractionation, J. Membr. Sci., 498 (2016) 192–200.
[37] Y. Lv, H.C. Yang, H.Q. Liang, L.S. Wan, Z.K. Xu, Novel nanofiltration membrane with ultrathin zirconia film as selective layer, J. Membr. Sci., 500 (2016) 265–271.
[38] R. Zhang, S. Ji, N. Wang, L. Wang, G. Zhang, J.R. Li, Coordination-driven in situ self-assembly strategy for the preparation of metal–organic framework hybrid membranes, Angew. Chem. Int. Ed., 53 (2014) 9775–9779.
[39] R. Zhang, Y. Su, X. Zhao, Y. Li, J. Zhao, Z. Jiang, A novel positively charged composite nanofiltration membrane prepared by bio-inspired adhesion of polydopamine and surface grafting of poly(ethylene imine), J. Membr. Sci., 470 (2014) 9–17.
[40] H. Vinh-Thang, S. Kaliaguine, Predictive models for mixed-matrix membrane performance: a review, Chem. Rev., 113 (2013) 4980–5028.
[41] Y.M. Zheng, S.W. Zou, K.G.N. Nanayakkara, T. Matsuura, J.P. Chen, Adsorptive removal of arsenic from aqueous solution by a PVDF/zirconia blend flat sheet membrane, J. Membr. Sci., 374 (2011) 1–11.
[42] H. Siddique, E. Rundquist, Y. Bhole, L.G. Peeva, A.G. Livingston, Mixed matrix membranes for organic solvent nanofiltration, J. Membr. Sci., 452 (2014) 354–366.
[43] T. Fukumoto, T. Yoshioka, H. Nagasawa, M. Kanezashi, T. Tsuru, Development and gas permeation properties of microporous amorphous TiO_2–ZrO_2–organic composite membranes using chelating ligands, J. Membr. Sci., 461 (2014) 96–105.
[44] G.I. Spijksma, C. Huiskes, N.E. Benes, H. Kruidhof, D.H.A. Blank, V.G. Kessler, H.J.M. Bouwmeester, Microporous zirconia–titania composite membranes derived from

diethanolamine-modified precursors, Adv. Mater., 18 (2006) 2165–2168.
[45] X.L. Wang, Y.Y. Fang, C.H. Tu, B. Van der Bruggen, Modelling of the separation performance and electrokinetic properties of nanofiltration membranes, Int. Rev. Phys. Chem., 31 (2012) 111–130.
[46] G.R. Xu, X.Y. Liu, J.M. Xu, L. Li, H.C. Su, H.L. Zhao, H.J. Feng, High flux nanofiltration membranes based on layer-by-layer assembly modified electrospun nanofibrous substrate, Appl. Surf. Sci., 434 (2018) 573–581.
[47] E. Bagheripour, A.R. Moghadassi, S.M. Hosseini, M.B. Ray, F. Parvizian, B. Van der Bruggen, Highly hydrophilic and antifouling nanofiltration membrane incorporated with water-dispersible composite activated carbon/chitosan nanoparticles, Chem. Eng. Res. Des., 132 (2018) 812–821.
[48] V. Vatanpour, S.S. Madaeni, R. Moradian, S. Zinadini, B. Astinchap, Novel antibifouling nanofiltration polyethersulfone membrane fabricated from embedding TiO_2 coated multiwalled carbon nanotubes, Sep. Purif. Technol., 90 (2012) 69–82.
[49] V. Vatanpour, M. Esmaeili, M.H.D.A. Farahani, Fouling reduction and retention increment of polyethersulfone nanofiltration membranes embedded by amine-functionalized multi-walled carbon nanotubes, J. Membr. Sci., 466 (2014) 70–81.
[50] S. Zinadini, A.A. Zinatizadeh, M. Rahimi, V. Vatanpour, H. Zangeneh, Preparation of a novel antifouling mixed matrix PES membrane by embedding graphene oxide nanoplates, J. Membr. Sci., 453 (2014) 292–301.
[51] H. Zhang, B. Li, J. Pan, Y. Qi, J. Shen, C. Gao, B. Van der Bruggen, Carboxyl-functionalized graphene oxide polyamide nanofiltration membrane for desalination of dye solutions containing monovalent salt, J. Membr. Sci., 539 (2017) 128–137.
[52] J. Miao, L.C. Zhang, H. Lin, A novel kind of thin film composite nanofiltration membrane with sulfated chitosan as the active layer material, Chem. Eng. Sci., 87 (2013) 152–159.
[53] Z. Song, M. Fathizadeh, Y. Huang, K.H. Chu, Y. Yoon, L. Wang, W.L. Xu, M. Yu., TiO_2 nanofiltration membranes prepared by molecular layer deposition for water purification, J. Membr. Sci., 510 (2016) 72–78.